

Available online at www.sciencedirect.com

jmr&t
Journal of Materials Research and Technology
journal homepage: www.elsevier.com/locate/jmrt



Achieving superior strength and ductility combination in Fe–28Mn–8Al–1C low density steel by orthogonal rolling

Yi Xiong ^{a,b,*}, Ze-wei Luan ^a, Xiao-qin Zha ^c, Yong Li ^d, Yun Yue ^a, Feng-zhang Ren ^a, Shu-bo Wang ^e, Wei Cao ^e

^a School of Materials Science and Engineering, Henan University of Science and Technology, Luoyang 471023, China

^b Provincial and Ministerial Co-construction of Collaborative Innovation Center for Non-ferrous Metal New Materials and Advanced Processing Technology, Luoyang 471023, Henan, China

^c Luoyang Ship Material Research Institute, Luoyang 471000, Henan, China

^d Central Iron and Steel Research Institute, Beijing 100081, China

^e Nano and Molecular Systems Research Unit, University of Oulu, FIN-90014, Finland

ARTICLE INFO

Article history:

Received 12 May 2023

Accepted 6 July 2023

Available online 12 July 2023

Keywords:

Low-density steel

Orthogonal rolling

Microstructure

Mechanical properties

ABSTRACT

Fe–Mn–Al–C austenitic steels have promising prospects for lightweight applications, due to their low density, excellent strength, and ductility. But the specific strength ratio of these alloys are still low as compared to other alloys. Herein, an orthogonal rolling (OR) process was used to improve the mechanical strength of a Fe–28Mn–8Al–1C low-density steel. The effect of this deformation method on the microstructural evolution and mechanical properties was studied by means of microscopy techniques, e.g. optic, scanning and transmission electron microscope, electron backscattered diffraction, X-ray diffraction, micro hardness and tensile test measurements. Microstructural characterization results show that OR significantly promotes the activation of multiple slip systems within grains in the material. The development of more uniform deformation microstructure, compared with that that after unidirectional cold rolling to the same strain was mainly due to the improvement of the uniformity of strain distribution by rolling deformation in multiple directions. It resulted in an average 84.5 nm sized ultrafine grain structures after 8-pass OR. The tensile and yield strengths were significantly increased to 1813 MPa and 1798 MPa, respectively. Despite of the still-existing strength-ductility trade-off, a much higher elongation at tensile failure of 9.6% was achieved, compared to only 5.2% of unidirectional cold rolled material. This superior strength and ductility combination was likely promoted by the increased dislocation density and deformation substructures in forms of dislocation cells, and deformation twins induced by OR.

© 2023 The Author(s). Published by Elsevier B.V. This is an open access article under the CC BY-NC-ND license (<http://creativecommons.org/licenses/by-nc-nd/4.0/>).

* Corresponding author. School of Materials Science and Engineering, Henan University of Science and Technology, Luoyang 471023, China.

E-mail address: xiongy@haust.edu.cn (Y. Xiong).

<https://doi.org/10.1016/j.jmrt.2023.07.059>

2238-7854/© 2023 The Author(s). Published by Elsevier B.V. This is an open access article under the CC BY-NC-ND license (<http://creativecommons.org/licenses/by-nc-nd/4.0/>).

1. Introduction

Fe–Mn–Al–C based low-density steels have attracted much attention in the field of lightweight steels, especially for the automotive industry, due to their low density, excellent strength and ductility [1–4]. According to alloy composition and phase composition at room temperature, Fe–Mn–Al–C low-density steel is divided into ferritic steel, austenitic steel and dual-phase steel, among which austenitic low-density steel has the most promising prospects, due to its outstanding weight reduction and unique deformation strengthening mechanism resulting from the addition of a large number of lightweight Al elements [5–8]. However, due to the rich slip system of the face-centered cubic (fcc) structure of austenite, the yield strength (YS) is relatively low, which limits its practical application in the engineering field [9]. Therefore, methods such as solid solution strengthening and precipitation hardening by adding alloying elements [10,11], grain refinement by cold rolling annealing and severe plastic deformation [12,13], and work hardening/deformation strengthening [14] are usually used to improve the mechanical properties of the alloy.

Introduction of high-density dislocations and grain refinement through plastic deformation is an effective way for strength enhancement in metallic materials [15,16]. Among these approaches, cold rolling is widely used, owing to its advantageous combination of high processing efficiency together with excellent dimensional accuracy and stable microstructure for final products [17,18]. For example, Ren et al. [14] reported the effect of cold rolling on the structure and properties of Fe–30Mn–11Al–1.2C steel, the results show that cold rolling can effectively increase the strength of low-density steel, but lead to a decrease in plasticity at the same time. After 90% rolling deformation, the yield strength of the material increases from 570 MPa without deformation to 2 GPa, while the elongation decreases to About 5%. Zhang et al. [19] and Mishra et al. [20] adopted the method of cold rolling followed by annealing to improve the adverse effect of cold rolling on the plasticity of low-density steel, but lead to a decrease in strength at the same time. An et al. [12] prepared Fe–28Mn–11Al–1C–5Ni low-density steel with high strength and plasticity combination by cold rolling and annealing, due to the fine grain strengthening caused by cold rolling and the B2 precipitation strengthening effect during the annealing process, 1.7 GPa tensile strength and 15% elongation were obtained finally. Cold rolling is an important link in the study of low-density strengthening and ductility of austenite. But the current research is carried out in the form of unidirectional rolling. Due to the use of a single strain in this rolling method, the activation of the slip system is limited, resulting in non-uniform plastic deformation [21]. Additionally, cold rolling also leads to strong texture, subsequent anisotropy in mechanical properties and reduced formability of rolled sheets which limits the wide application of cold rolled materials in industry [22].

To improve the adverse effect of cold rolling deformation on materials and obtain better microstructure uniformity and mechanical properties, the current rolling process is to change the rolling direction by introducing an additional cross-rolling

step in the deformation process [23,24]. It has been reported that deformation Changes in the route will affect the sub-structure formed in the previous step, therefore, changing the rolling route will have a significant impact on the crystal texture, microstructure and mechanical properties of the material [25]. For example, Mohammadzahi et al. [26] compared the effects of ordinary cold rolling and cross rolling on AISI 316 austenitic stainless steel, and the results showed that cross-rolling has a high potential for the enhancement of mechanical properties at low thickness reductions, preservation of equiaxed structure even at high thickness reductions, and decreasing of anisotropy and directionality of properties. In addition, cross-rolling will also promote the activation of the slip system and obtain a more uniform deformation structure. For example, Tian et al. [27] used cross-rolling to promote the activation of non-substrate slip during plastic deformation and improved the Mg alloy sheet. Formability prepared a rare earth magnesium alloy plate with no cracks and good plasticity. However, the current research on cross-rolling is all rotating around the ND direction, which is still a unidirectional compression in essence, so the activation effect on the slip system is limited, and the grain refinement effect is not obvious. On the other hand, multi-direction forging is a common method to prepare fine structures [28,29]. For example, Shahriyari et al. [30] employed this method to prepare Cu–Zn alloy with a uniform and fine grain structures ($\leq 1 \mu\text{m}$). Investigation by Sakai et al. [31] showed that this method accelerated the intersection or torsion of shear bands in different directions, thus leading to the development of ultrafine crystal structure. However, the process is only suitable for metals with low deformation resistance, such as aluminum alloy [32], copper alloy [33], magnesium alloy [34], low carbon steel [35], etc.

In the present paper, this work draws on the advantages of multi-directional forging and cross-rolling to design an orthogonal rolling deformation on Fe–28Mn–8Al–1C low-density steel. The aim is to effectively obtain uniform and fine structures by changing the rolling path and planes in multiple directions to facilitate the activation of the slip systems in materials at room temperature. Comprehensive characterizations and measurements were carried out to explore the effect of this plastic deformation approach on the microstructure evolution and subsequently on the mechanical properties of the low-density steel.

2. Materials and experimental procedures

Low-density Fe–28Mn–8Al–1C (in wt%) steel was firstly prepared casting after melting the raw ingredients in a vacuum induction furnace. The density of as-cast ingot was measured to be 6.82 g/cm^3 using the Archimedean principle. After casting, the ingo was heated to $1200 \text{ }^\circ\text{C}$ for 2 h, followed by hot forging to billets with a cross section of $100 \text{ mm} \times 100 \text{ mm}$. Four group of samples with a dimension of $8 \times 8 \times 100 \text{ mm}^3$ for orthogonal rolling (OR), and one group sample with a thickness of 5 mm for unidirectional cold rolling (CR) were cut from center of the forged billets the forging direction. Before rolling, all samples were treated by solution treatment at $1000 \text{ }^\circ\text{C} \times 1 \text{ h}$ followed by water quenching to room temperature. A LG-300

three-phase asynchronous two-high mill was used to carry out OR in which 1 pass OR deformation occurred in multiple planes: the RD (rolling direction)-TD (transverse direction) plane and RD-ND (normal direction) plane by 90° rotation about RD, as schematically shown Fig. 1. RD, TD and ND were designated by referring to the very first rolling pass. Finally, samples after 2, 4, 6, 8 OR passes were obtained. The commercial Forge software was used to simulate the OR process to obtain the equivalent strain values. More OR and simulation details can be found in our previous work [36]. The modelled equivalent strain values for 2, 4, 6, 8 OR passes were 0.43, 0.83, 1.25 and 1.62, respectively. One group of samples were prepared by unidirectional CR to a total thickness reduction of 80%, for comparative analysis of microstructure and mechanical properties. The achieved true strain was 1.6, similar the equivalent strain, 1.62 of 8 passes OR.

Samples for optical microscope metallographic observation were prepared by grinding and polishing step by step following the metallographic sample preparation methods. An OLYMPUS PMG3 optical microscope was used for imaging the etched surface of specimens. The etchant was 5 g copper chloride dissolved in 100 ml hydrochloric acid and 100 ml ethanol solution. Samples for EBSD were prepared by electrolytic polishing in an electrolyte that was composed of 5% perchloric acid and 95% (vol.%) acetic acid. The applied voltage was 50 V and polishing time was 30 s, respectively. TEM thin foils was finally thinned by Gatan 691 ion thinning instrument and then observed by JEM-2010 TEM operating at 200 keV. X-ray diffraction (XRD) profiles for phase composition and microstrain analysis were collected in 30°–100° range by D8 ADVANCE X-ray diffractometer equipped with Cu-K α X-ray source (wavelength $\lambda = 0.15406$ nm).

The hardness of samples were measured using a HV-1000 microhardness tester, and were the average of at-least 5 measurements of each sample. Tensile specimens, with dimension shown in Fig. 2 Were machined flat from the rolled materials along RD. The mechanical properties at room temperature were then determined by tensile tests using Instron

5587 tensile testing machine with a tensile speed of 0.2 mm/min. After tensile failure, JSM-7800F FESEM was employed to observe the fracture surface morphology.

3. Results

3.1. Microstructure evolution

3.1.1. Optical microscope characterizations

Fig. 3(a) shows that the undeformed Fe–28Mn–8Al–1C low-density steel possesses equiaxed grain structure with an average grain size of about 40.3 μm . A small amount of annealing twins can also be clearly observable. After 2-pass OR at a strain level of 0.43, the grains, viewed at the ND-TD plane, remain equiaxed (Fig. 3(b)), which become elongated along RD (Fig. 3(c)). A lot of slip bands appear. The grains become further elongated, while the number of slip bands increases but the inter-slip band spacing decreases gradually with increase in OR passes. It is worth noting that slip bands orient roughly 45° to RD at lower strains (Fig. 3(c) (e) for 2 and 4 pass OR). This direction represents the direction of maximum shear stress during OR. In some grains, it can be found that two differently oriented slip bands intersect each other, which is attributed to the activation of different slip systems by multiple changes in the direction of applied rolling force. These slip bands are almost indistinguishable, while the slip bands perpendicular to RD appears after 6-pass OR as shown in the rectangular region in Fig. 3(h). Further increasing OR to 8 passes, the deformed grains change from flat to banded shapes, and number of slip bands further increase. Those present slip bands are oriented either parallel with RD (elliptic region in Fig. 3(i)) or perpendicular to RD (rectangular region in Fig. 3(i)). On the other hand, the microstructure of unidirectional CR low-density steel is completely different in Fig. 3(j). Due to the action of rolling force in a single direction, the equiaxed grains are compressed into flat shape, and the direction of developed slip bands is mainly parallel to ND.

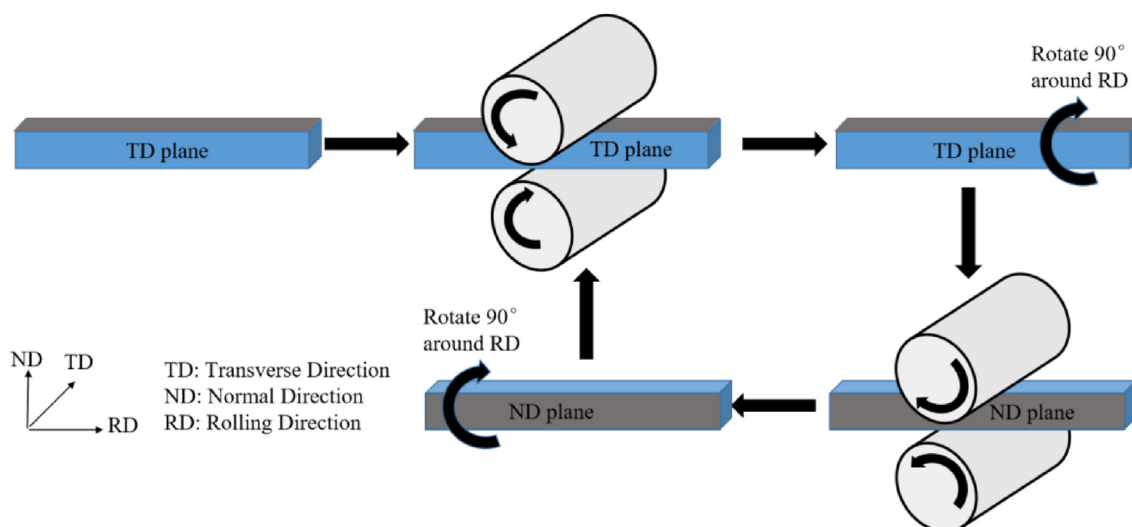


Fig. 1 – Schematic diagram of individual orthogonal rolling pass. RD, TD, ND refers to the first rolling pass, i.e. the left panel.

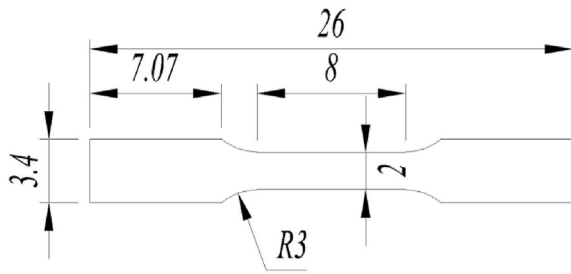


Fig. 2 – Dimensions (in mm) of the tensile specimens (thickness: 1 mm).

3.1.2. TEM observations

More microscopic details about the OR deformed microstructures are examined and illustrated by TEM, as shown in Fig. 4. Under lower strain of 0.43 (2 pass OR), the ORed microstructure in Fig. 4(a) exhibits a significant amount of planar slip bands, in which the co-planar slip bands are parallel to each

other while non-coplanar ones intersecting with each other. This leads to the formation of Taylor lattice [37]. At these intersections, dislocations are seen to accumulate. Moreover, the slip bands develop through the entire grain until impinge on grain boundaries, revealing relatively weak interactions between these intersecting slip bands. After 4-pass OR (Fig. 4(b)), there is not obvious microstructural changes compared with Fig. 4(a), but the spacing between slip bands reduces significantly and dislocation pile-ups at the slip band intersections increase. Quantitatively, the average slip band spacing reduces from 312 nm at 2-pass to 140 nm at 4-pass OR.

After 6-pass OR (Fig. 4(c)), the slip bands formed by the slip of the dislocation plane gradually disappears, and the dislocation wall and dislocation cell begin to be observed, which means that the dislocation cross slip is activated. Dislocation density increases significantly after 8-pass OR, as unveiled in Fig. 4(d). Meanwhile, dislocation entanglements and cells are observed also to form in localized regions. The aforementioned features of planar slip bands disappear

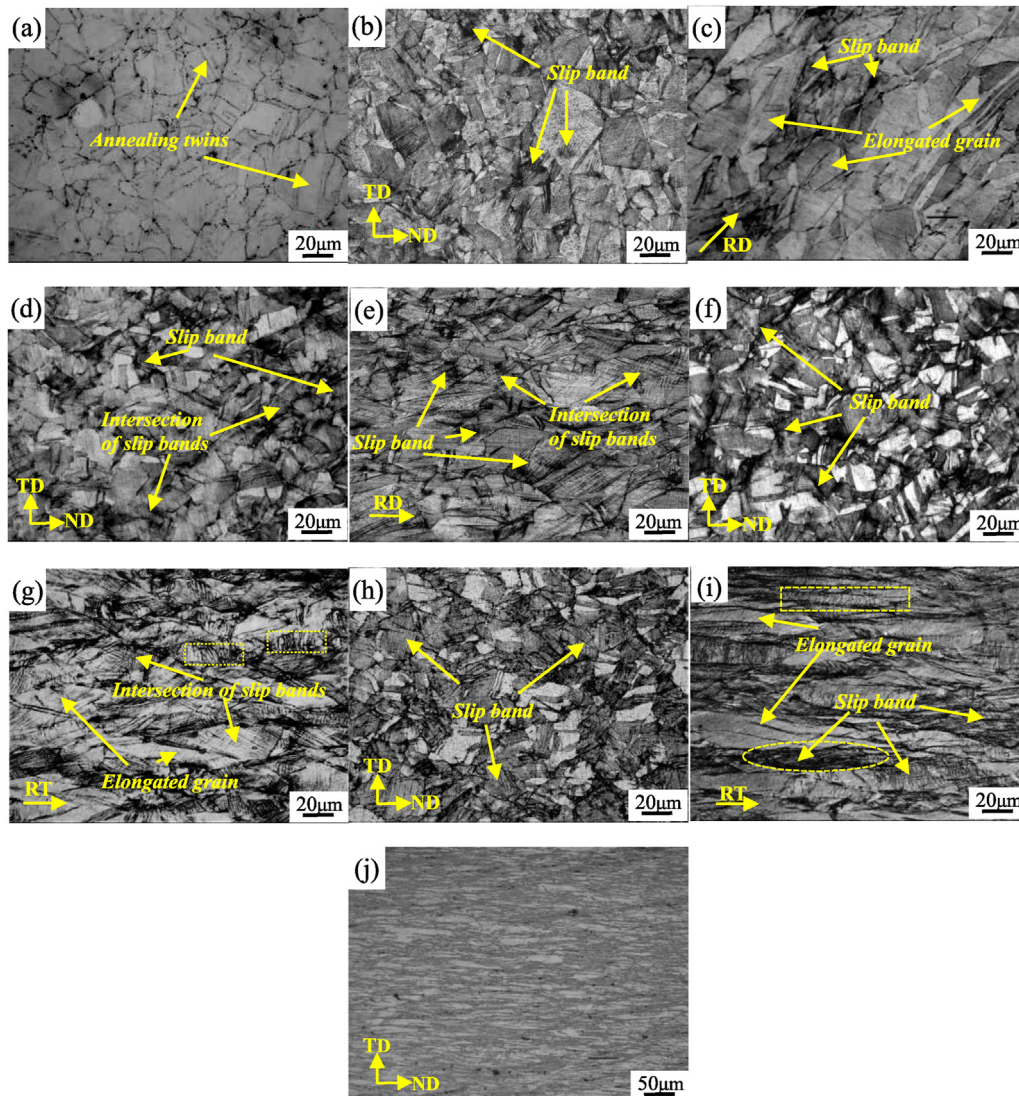


Fig. 3 – Optical microscope images for Fe–28Mn–8Al–1C low-density steels: (a) before OR; after (b–c) 2 pass OR; (d,e) 4 pass OR; (f,g) 6 pass OR; (h,i) 8 pass OR; and (j) after unidirectional CR to 80% thickness reduction.

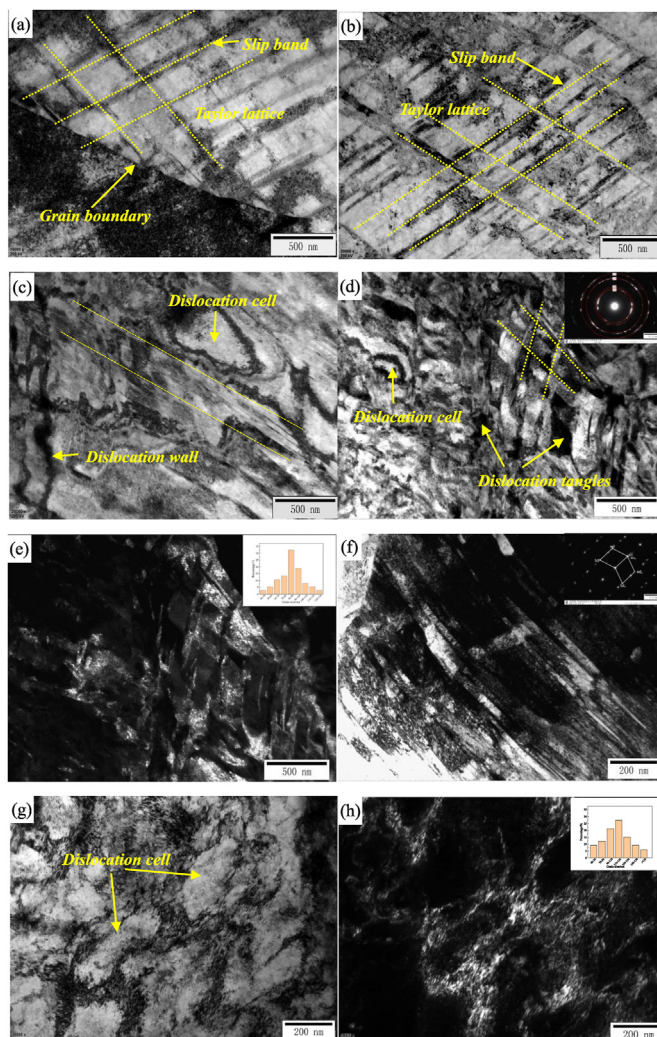


Fig. 4 – TEM images of Fe–28Mn–8Al–1C low-density steels after: (a) 2-pass OR; (b) 4-pass OR; (c) 6-pass OR; (d) BF-TEM image for 8-pass ORed steel; (e) corresponding DF-TEM of (d); (f) BF-TEM image of nanotwins in 8-pass ORed steel; (g) after unidirectional CR for a 80% reduction; (h) corresponding DF-TEM of (g).

in this case. Quantitative analysis of the corresponding DF-TEM image reveals an average grain size of 84.5 nm, presenting significant grain refinement by 8-pass OR. Resultant selected area electron diffraction pattern (SAED) appears to be a relatively continuous ring, suggesting that these nano-scale grains have multiple orientations. Nanotwins have also been found in some grains, as representatively illustrated in Fig. 4(f). Indexation of the corresponding SAED indicated twins. As a comparison, mainly dislocation cells form in the 80% unidirectional cold rolled steel Fig. 4(g), which is a typical dislocation structure developed by dislocation cross-slip. Quantitative analysis of the corresponding DF-TEM image reveals an average grain size of 119.4 nm.

3.1.3. XRD analysis

Fig. 5 (a) reveals that the Fe–28Mn–8Al–1C low-density steel before any OR or unidirectional CR has single austenitic (γ) phase. Deformation induced martensitic transformation is not detected after OR nor comparative unidirectional CR,

suggesting a good phase stability of such high-Mn low-density steel with high Al content. However, the diffraction peaks are observed to become broader with increase in OR passes. Taking the diffraction peak of austenitic (220) plane as an example, the full-width at half maximum (FWHM) of it for the 8-pass ORed sample has broadened to 1.011° , compared with 0.502° of that for the undeformed counterpart in Fig. 5(b). Williamson-Hall method points out that the broadening of diffraction peak is caused by both grain refinement and microscopic strain, which can be expressed by [38,39]:

$$\beta_r = \frac{K\lambda}{D \cos \theta} + 4\epsilon \tan \theta \quad (1)$$

where $K\lambda/(D\cos\theta)$ is the broadening contribution resulted from significant grain refinement, in which $K (= 0.9)$, λ (0.15406 nm), D and θ are the shape factor, wavelength of the X-ray source, grain size and peak position in radians, respectively. $4\epsilon \tan\theta$ represents the peak broadening induced by microstrain ϵ . Through careful fitting analysis, the calculated microstrains of

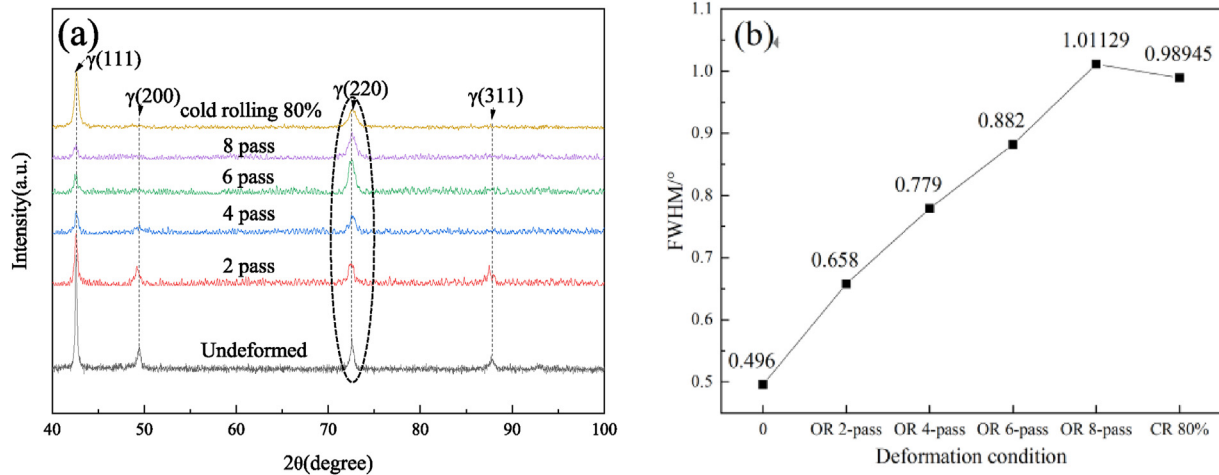


Fig. 5 – XRD patterns of Fe–28Mn–8Al–1C low density steels. (a) XRD profiles; (b) FWHM of representative austenitic (220) peak.

the initial and rolled samples are shown in Fig. 6. It is seen that the microstrain gradually increases to 6.1×10^{-3} after 8-pass OR, which is 2.2 times of the initial sample that is 2.8×10^{-3} . Correspondingly, dislocation density can be calculated by [40]:

$$\rho = \frac{2\sqrt{3}\epsilon}{Db} \quad (2)$$

where ϵ is the average microstrain, b is the modulus of Burgers vector. The calculated dislocation densities are also illustrated in Fig. 6, which is $3.2 \times 10^{14}/\text{m}^2$ for the undeformed (0-pass) sample and then increases to $2.84 \times 10^{15}/\text{m}^2$ after 8-pass OR. Unidirectional CR can also greatly promote the dislocation density in this low-density steel that is $1.5 \times 10^{15}/\text{m}^2$ at similar strain level around 1.6. However, this is much lower than, only about 53% of that for the 8-pass ORed sample.

3.1.4. EBSD analysis

Fig. 7 show the inverse pole figure (IPF) with corresponding pole figure, and grain boundary orientation histogram of the low density steels. Prior to rolling, the material consists of randomly oriented equiaxed grains with an average grain size of 43 μm and a few annealed twins. Consequently, it is seen

that HAGBs dominate, accounting for 94.65% in the material. After 2-pass OR, the grain size decreases significantly to 17.8 μm , but the grain shape still remain equiaxed. Meanwhile, the fraction of LAGBs starts to increase and grain orientation starts to converge, which results in a maximum texture strength of 2.55 (Fig. 7(b)). The grain size has been further reduced to 12.3 μm due the appearance of a small number of broken grains, when the OR passes increase to 4. Texture becomes stronger, as the maximum texture strength increases to 3.19 (Fig. 7(c)). After 8-pass OR (Fig. 7(d)), those initial equiaxed grains break into a large number of fine ones, resulting in the development of $\{110\}<100>$ Gaussian texture with a maximum texture strength of 4.18. Moreover, the proportion of HAGBs decreases to 2.36% and the LAGBs ratio increases to 97.64%. On the contrary, elongated grains along RD with also broken grains are found in the 80% unidirectional CR sample (Fig. 7(e)). The developed deformation texture mainly consists of a $\{110\}<112>$ brass type texture component with a maximum strength of 4.4. In addition, the specimen possess a lower fraction of LAGBs, about 92.64%, than that after 8-pass OR.

3.2. Mechanical properties

3.2.1. Strength and elongation

Fig. 8(a) shows the tensile strength, yield strength, and elongation at tensile failure of Fe–28Mn–8Al–1C low-density steels extracted from experimental engineering stress–strain curves that representatively present in Fig. 8(b). The undeformed sample has a hardness, tensile strength, yield strength, and elongation of 284 Hv, 882 MPa, 505 MPa, and 64%, respectively, giving a yield-to-tensile strength ratio of 0.57. The strength and hardness gradually increase with the increase of OR passes. After 8-pass OR, the hardness, tensile strength and yield strength have increased to 545 HV, 1813 MPa and 1798 MPa, i.e., an increase of 92%, 106% and 254%, respectively. However, the elongation has decreased to 9.6%. Nevertheless, this enhancement in comprehensive mechanical properties is seen to be much better than that of the unidirectional CR sample to a similar strain of 1.6 with

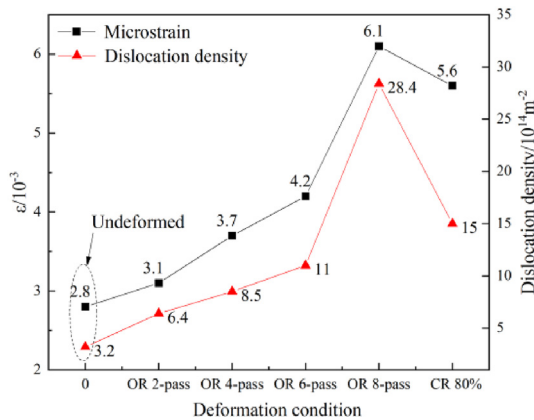


Fig. 6 – Calculated microstrain and dislocation density of Fe–28Mn–8Al–1C low-density steel.

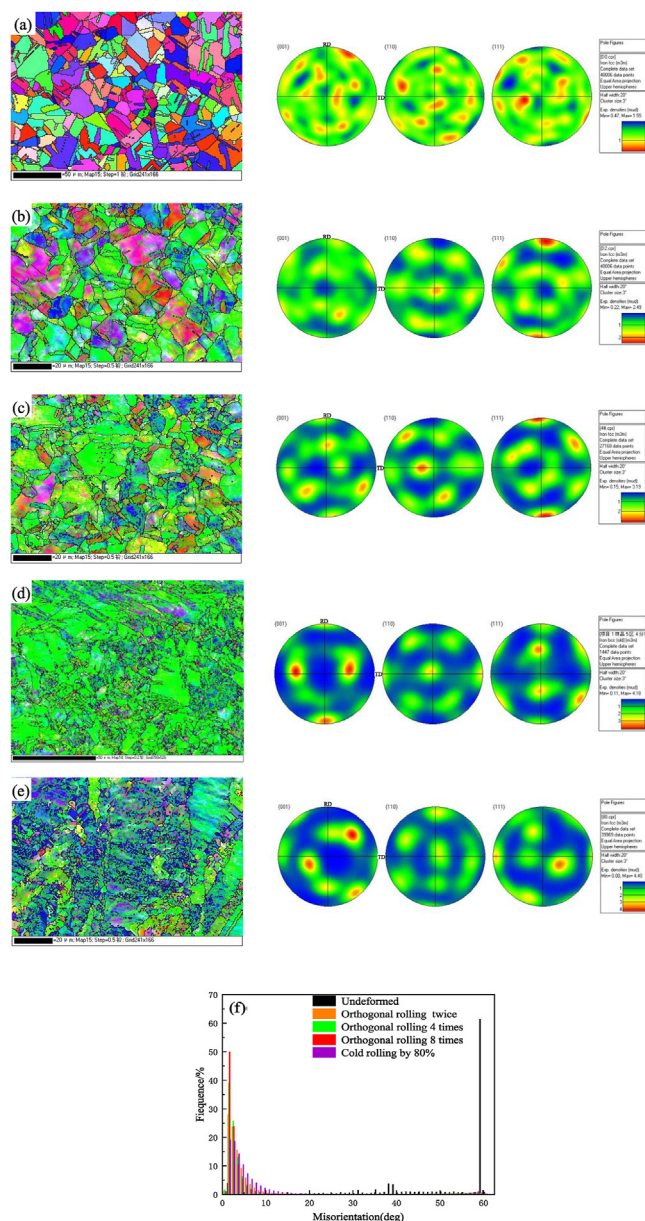


Fig. 7 – IPF mapping and PF of Fe–28Mn–8Al–1C low-density steel: (a) undeformed; (b) OR 2 passes; (c) OR 4 passes; (d) OR 8 passes; (e) CR 80%; (f) Comparison of low and high angle grain boundaries. In the IPF maps, the solid black, and green lines depict the high and low angle grain boundaries (HAGBs, $>15^\circ$) and low angle grain boundaries (LAGBs, $\leq 15^\circ$).

yield strength of 1603 MPa, tensile strength 1688 MPa and elongation of only 5.2%.

3.2.2. Fractography

Fig. 9(s) shows the fracture surface of undeformed Fe–28Mn–8Al–1C low-density steel is characterized by large and deep dimples, indicating that the specimen has good plasticity. Such a feature is consistent with the 65% elongation of this sample. The dimples become smaller and flatter for 2-pass ORed sample in Fig. 9(b), compared with undeformed

one. It is seen that the size and depth of dimples decreases with further increase in OR passes, while the distribution of dimples become more dense and uniform, indicating that ductile fracture is still dominant. After 8-pass OR, the average diameter of dimples is measured to only $0.62 \mu\text{m}$, corresponding to a relatively low macroscopic fracture elongation of 9.6%. Differently, flat dimples and a small number of cleavage planes can be observed for the 80% cold rolled sample in Fig. 9(f), showing the characteristic of a mixed ductile-brittle fracture with low elongation of only 5.2%.

4. Discussion

The microstructural evolution of Fe–28Mn–8Al–1C low-density steel during OR is characterized by multiple stages, i.e., planar slip of dislocations occurring at low strains, and following wave slip with increasing deformation, which is consistent with the previous study on the microstructural evolution of Fe–30Mn–11Al–1.2C low-density steel subjected to conventional CR [14]. However, comparing the microstructures after 8-pass OR and CR 80% with the same equivalent strain (Fig. 4), part of the dislocation planar slip still retains after 8-pass OR, which evolves into dislocation cells after CR. This may be related to the activation capability of slip systems by different rolling methods. It is known that the applied resolved shear stress on slip systems of individual grain is different due to grain orientations during plastic deformation of polycrystalline materials, leading to a varying degree of difficulty to realize homogeneous deformation [41,42]. During unidirectional CR, the material is subjected to single direction of rolling force. The activation of slip system, thus, is limited, i.e., the grains with soft orientation are preferentially and firstly involved in deformation, while the hard-oriented grains must be rotated and/or twinned to develop a favorable orientation for deformation [41,43]. Thus, unidirectional rolling is easy to trigger increased dislocation cross-slip, leading to dislocation interactions and the formation of dislocation walls and cells, and other sub-structures.

In contrast, OR can apply rolling forces in multiple directions by repeatedly changing rolling planes, which can activate more slip systems to participate in plastic deformation and also reduce non-essential grain rotations. Therefore, OR promotes the development of slip bands with multiple orientations (Fig. 4) and results in more low-angle grain boundary angles (Fig. 7) in the investigated steel. For high Mn–Al–C austenitic low-density steels, the transition from dislocation plane slip to wave slip is owing to the hardening of slip plane [44], resulting from the dislocation multiplication and pileup within the slip plane. With increasing deformation, wave slip of dislocations occurs, either when the dislocations on parallel slip bands are close enough to annihilate, or when the increasing stresses make cross slip possible. Thus, higher strains is needed to realize the change of dislocations move from plane slip to cross slip, attribute to the activation of more slip systems.

For deformation of metals and alloys with fcc crystal structure, the first stage, easy slip, only present in single crystals, but the second, rapid hardening stage and third, dynamic recovery stage dominate in polycrystalline materials

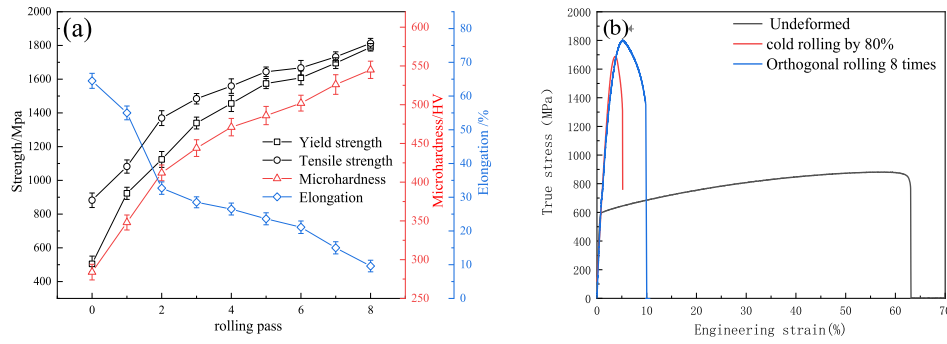


Fig. 8 – Mechanical properties of the Fe–28Mn–8Al–1C low-density steel: (a) Yield and tensile strength, and elongation and hardness as a function of OR passes; (b) Representative engineering stress–strain curves for undeformed, 8-Pass OR and unidirectional CR samples.

[45]. The second stage is characterized by a monotonic increase in the density of stored dislocations, resulting in rapid hardening; the dynamic recovery stage produces cross-slip of dislocations, forming cellular sub-structures and gradual decrease in hardening rate [46]. In this study, it is found that OR promotes the development of slip bands so that dislocation wave slip is activated at higher strain conditions. This facilitates the reduction of dynamic reversion of dislocations during plastic deformation, and therefore the ORed sample possess higher dislocation density than that unidirectional CR at the same equivalent strain condition, like the findings in 316L stainless steel [26]. In addition, the slip bands with different orientations intersect each other due to the change of the direction of the applied load, resulting in grain fragmentation, which fully develops into a new grain structure under the subsequent high cumulative strain. Therefore, the grain refinement effect of orthogonal rolling is more significant than that of ordinary cold rolling.

Based on the above analysis, the significant increase of dislocation density and grain refinement caused by orthogonal rolling will have a significant impact on the mechanical properties of Fe–28Mn–8Al–1C low-density steel. Studies have shown that solid solution strengthening (σ_{SS}), dislocation strengthening (σ_D), grain boundary strengthening (σ_{GB}) and secondary phase strengthening (σ_{SP}) are the main methods to improve the strength (σ) of metal materials [41]. Usually, the theoretical strength of materials can be determined by etc. (3) expression:

$$\sigma = \sigma_{SS} + \sigma_D + \sigma_{GB} + \sigma_{SP} \quad (3)$$

where, σ_{SS} , σ_D , σ_{GB} , and σ_{SP} are the contributions of solid solution strengthening, dislocation strengthening, fine grain strengthening and second phase strengthening to the tensile strength of the material, respectively. Among them, the increase of dislocation density and grain refinement during the rolling deformation process are the main reasons for the

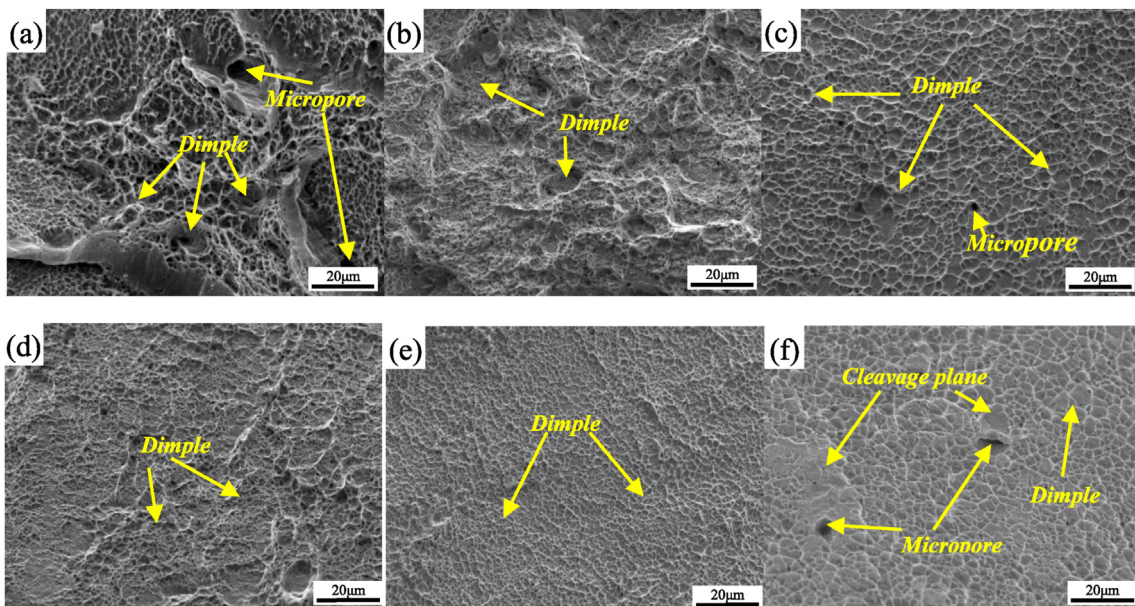


Fig. 9 – Fracture surfaces of the Fe–28Mn–8Al–1C low-density steel: (a) undeformed; (b) OR 2 passes; (c) OR 4 passes; (d) OR 6 passes; (e) OR 8 passes; (f) CR 80%.

increase of material strength. High-density dislocations will provide significant dislocation strengthening for the material. According to Taylor hardening law, the yield strength of the material is proportional to the square root of the dislocation density. The strengthening effect can be evaluated according to the Taylor hardening equation [47]:

$$\sigma_D = MaGb\sqrt{\rho} \quad (4)$$

where, $M = 3.06$ [48] is the Taylor factor of randomly distributed grain orientation, $a = 0.23$ [48] is the empirical strength coefficient, $G = 67.3$ GPa [48] is the shear modulus of the material, $b = 0.286$ nm [48] is the Burgers vector, ρ is the dislocation density of material, as shown in Fig. 6, the calculation results show that the enhancement effect of dislocation strengthening on the strength of OR8 passes and CR80% is 722 MPa and 524 MPa, respectively.

Grain refinement is another important factor leading to the improvement of material strength. During plastic deformation process, grain boundaries are effective barriers to hinder dislocation movement. The smaller the grain size, the more the grain boundaries, and the more significant the strengthening effect, the grain refinement also helps to reduce stress concentration effects during plastic deformation, and the recognized grain refinement effect is often evaluated by the Hall–Petch equation [19]:

$$\sigma_{GB} = \sigma_0 + K_y d^{-1/2} \quad (5)$$

where σ_0 is the contribution of lattice friction stress and solid solution strengthening of alloying element ($\sigma_0 = 97 + 279\text{wt}\% \text{C} + 1.5\text{wt}\% \text{Mn} + 20.5\text{wt}\% \text{Al}$, in MPa [19]), $k_y = 461$ MPa/ $\mu\text{m}^{1/2}$ [19] is a material constant, and d represents the grain size. Note here that since the grains are not equiaxed after rolling deformation, the grain size available for calculation should be corrected according to the grain geometry. For example, the geometry factor along the flattened grains of a large strain plate after rolling is about 1.4. The calculation results show that the contribution of grain refinement to strength after OR8ed and CR80% is 1442 MPa and 1229 MPa. The theoretical yield strengths of the low-density steel after OR8ed and CR80% cold rolling are 2164 MPa and 1753 MPa, which are 366 MPa and 150 MPa different from the experimental values. The reason may be related to a certain deviation in the Hall–Petch relationship when the grain size is in the nanometer range, Jiang et al. [13] also showed a similar research phenomenon on Fe–Mn–Al–C low-density steel after high-pressure torsion. In summary, the combined effect of increased dislocation density and grain size refinement caused by rolling deformation leads to higher strength of ORed specimens.

The ORed Fe–28Mn–8Al–1C low-density steels exhibits the common strength-ductility tradeoff dilemma. The refined grains improve strengths but prevents effective storage of dislocations within grains. Moreover, high initial dislocation density in deformed materials provides little room for further accumulation of dislocations as well as low strain hardening capacity [49]. However, compared with conventional rolling, the ORed specimens exhibited a more excellent balance of strength and plasticity under the same equivalent strain, which may be due to the following two reasons: One is that OR

promotes the activation of more slip systems, increases the dislocation storage capacity in the material and makes the material have certain strain hardening ability and better ductility. The second is that orthogonal rolling leads to the activation of nanotwins, forming a heterostructure composed of ultrafine grains and nanotwins. Previous studies have shown that nano-twin boundaries have a unique strengthening effect compared with ordinary grain boundaries. The introduction of nano-twins in ultrafine-grained metals can not only provide higher strength, but also hardly sacrifice the ductility of the metal [50]. The enhanced strain hardening ability is attributed to the coherence of twin boundaries. Since the twin boundary is a special low-energy coherent grain boundary, the interaction between dislocations and twin boundaries is fundamentally different from the interaction between dislocations and grain boundaries in polycrystalline materials [51]. When dislocation slip encounters a grain boundary, it will be strongly resisted by the grain boundary and stress concentration will be generated at the grain boundary. Due to the disordered structure of the grain boundary, it is difficult for dislocations to move and store effectively at the grain boundary, resulting in an increase in strength but a decrease in ductility. However, coherent twin boundaries can not only act as grain boundaries to hinder the movement of dislocations, but also serve as sources and/or sinks of dislocations, and twin boundaries can act as slip planes on which dislocations can move and stack, therefore, the stress concentration at the dislocation-twin intersection can be effectively released by the dislocation slip along the twin boundary [52]. Therefore, the plastic deformation stability and work hardening ability of low-density steels are improved by introducing nano-twins in metals with ultrafine-grain structure, resulting in high strength and plasticity.

5. Conclusions

In this work, microstructural evolution and mechanical properties of Fe–28Mn–8Al–1C low-density steel subjected to orthogonal rolling have been investigated. The 8-pass ORed samples have also been studied in contrast with the unidirectional cold rolled ones to a same equivalent strain. Following conclusions can be drawn.

1. Due to the repeatedly changing of applied force during OR, the activation of multiple slip system is more obvious and the stored dislocation density after OR increases significantly.
2. A more homogeneous fine-grained structure after OR has been observed, compared to conventional unidirectional cold rolling. An average grain size of 84.5 nm is developed after 8-pass OR. This grain refinement is attributed to the dislocation interaction as well as interaction between dislocations and twins.
3. The yield strength and ultimate tensile strength of the 8-pass ORed steel are remarkably increased up to 1798 MPa and 1813 MPa, respectively. Compared with conventional CR, multiple slip systems, twins and high-density stored dislocations can be activated during OR, which promotes a

more significant improvement of the mechanical properties of steel.

4. Fractography observation reveals that ductile dimple fracture still dominates in this heavily deformed material, achieving an elongation of 9.6% that is much higher than that of 5.2% of unidirectional rolled steel with a mixed ductile-brittle fracture. The deformation twins and more slip systems can provide extra room to accommodate more dislocations while hindering dislocations movements. Therefore, a good combination of strength and ductility can be obtained after 8-pass OR.

Declaration of Competing Interest

The authors declare that they have no known competing financial interests or personal relationships that could have appeared to influence the work reported in this paper.

Acknowledgments

This work was supported by the National Natural Science Foundation of China (Grant No. U1804146, 51905153, and 52111530068); the Science and Technology Innovation Team of Henan University of Science and Technology (Grant No. 2015XTD006) and Major science and technology projects of Henan Province (Grant No. 221100230200).

REFERENCES

- [1] Chen S, Rana R, Haldar A, Ray RK. Current state of Fe-Mn-Al-C low density steels. *Prog Mater Sci* 2017;89:345–91.
- [2] Zambrano OA. A general perspective of Fe–Mn–Al–C steels. *J Mater Sci* 2018;53(20):14003–62.
- [3] Chen L, Zhao Y, Qin X. Some aspects of high manganese twinning-induced plasticity (TWIP) steel, a review. *Acta Metall Sin (Engl Lett)* 2013;26(1):1–15.
- [4] Gutierrez-Urrutia I. Low density Fe–Mn–Al–C steels: phase structures, mechanisms and properties. *ISIJ Int* 2021;61(1):16–25.
- [5] Mishra B, Mukhopadhyay A, Sarkar R, Kumawat MK, Madhu V, Prasad MJNV. Strain hardening and stored energy in high-Mn austenitic based low-density steel. *Mater Sci Eng* 2022;861:144331.
- [6] Ding H, Liu D, Cai M, Zhang Y. Austenite-based Fe-Mn-Al-C lightweight steels: research and prospective. *Metals* 2022;12(10):1572.
- [7] Shi HY, Zhang GF, Tang YH, Man W, Ji PF, Zhang XY, et al. Microstructure and mechanical properties of a Fe–30Mn–10Al–1.5 C–x Be (x= 0, 0.5, 1.0, 1.5) Be low-density steels. *Mater Char* 2023;112643.
- [8] Moon J, Park SJ, Jang JH, Lee TH, Lee CH, Hong HU, et al. Investigations of the microstructure evolution and tensile deformation behavior of austenitic Fe-Mn-Al-C lightweight steels and the effect of Mo addition. *Acta Mater* 2018;147:226–35.
- [9] Sarma VS, Wang J, Jian WW, Kauffmann A, Conrad H. Role of stacking fault energy in strengthening due to cryo-deformation of FCC metals. *Mater Sci Eng* 2010;527(29–30):7624–30.
- [10] Banis A, Gomez A, Bliznuk V, Dutta A, Sabirov I, Petrov RH. Microstructure evolution and mechanical behavior of Fe–Mn–Al–C low-density steel upon aging. *Mater Sci Eng* 2023;875:145109.
- [11] Xie Z, Hui W, Zhang Y, Zhao XL. Effect of Cu and solid solution temperature on microstructure and mechanical properties of Fe-Mn-Al-C low-density steels. *J Mater Res Technol* 2022;18:1307–21.
- [12] An YF, Chen XP, Ren P, Cao WQ. Ultrastrong and ductile austenitic lightweight steel via ultra-fine grains and heterogeneous B2 precipitates. *Mater Sci Eng* 2022;860:144330.
- [13] Jang G, Kim JN, Lee H, Lee T, Enikeev N, Abramova M, et al. Microstructural evolution and mechanical properties of nanocrystalline Fe–Mn–Al–C steel processed by high-pressure torsion. *Mater Sci Eng* 2021;827:142073.
- [14] Ren P, Chen XP, Wang CY, Cao WQ, Liu Q. Evolution of microstructure, texture and mechanical properties of Fe–30Mn–11Al–1.2 C low-density steel during cold rolling. *Mater Char* 2021;174:111013.
- [15] Sohn SS, Song H, Suh BC, Kwak JH, Lee BJ, Kim NJ, et al. Novel ultra-high-strength (ferrite+austenite) duplex lightweight steels achieved by fine dislocation substructures (Taylor lattices), grain refinement, and partial recrystallization. *Acta Mater* 2015;96:301–10.
- [16] Lima MNDS, Loureiro RCP, Béres M, Masoumi M, Munoz JC, Rodrigues SF, et al. Influence of cold deformation on microstructure, crystallographic orientation and tensile properties of an experimental austenitic Fe–26Mn-0.4C steel. *J Mater Res Technol* 2022;19:7–19.
- [17] Wang PF, Jie JC, Liu CB, Guo LJ, Li TJ. An effective method to obtain Cu-35Zn alloy with a good combination of strength and ductility through cryogenic rolling. *Mater Sci Eng* 2018;715:236–42.
- [18] Wu H, Tan Y, Malik A, Wang YW, Naqvi SZH, Cheng HW, et al. Dynamic compressive mechanical behavior and microstructure evolution of rolled Fe-28Mn-10Al-1.2 C low-density steel. *Materials* 2022;15(10):3550.
- [19] Zhang G, Ma W, Tang Y, Wang F, Zhang X, Wang Q, et al. Investigation on the microstructural evolution and mechanical properties of partially recrystallized Fe-27Mn-10Al-1.4 C steel. *Mater Sci Eng* 2022;833:142545.
- [20] Mishra B, Sarkar R, Singh V, Kumar D. Effect of cold rolling and subsequent heat treatment on microstructural evolution and mechanical properties of Fe-Mn-Al-C (Ni) based austenitic low-density steels. *Mater Sci Eng* 2022;861:144324.
- [21] Faraji G, Kim HS, Kashi HT. Severe plastic deformation methods, processing and properties. Amsterdam: Elsevier Science; 2018. p. 113–29 [Chapter 3], Severe plastic deformation methods for sheets.
- [22] Lee NS, Chen JH, Kao PW, Chang LW, Tseng TY, Su JR. Anisotropic tensile ductility of cold-rolled and annealed aluminum alloy sheet and the beneficial effect of post-anneal rolling. *Scripta Mater* 2009;60(5):340–3.
- [23] Rout M, Pal SK, Singh SB. Cross rolling: a metal forming process. In: *Modern manufacturing engineering*. Springer; 2015. p. 41–64.
- [24] Ma K, Elgallad EM, Chen ZX, Xiao BL, Chen XG. Improving the elevated-temperature mechanical properties of AA3004 hot-rolled sheets by microalloying with Mo and optimizing the process route. *J Mater Res Technol* 2022;19:4489–503.
- [25] Mohammadzahi S, Mirzadeh H. Cold unidirectional/cross-rolling of austenitic stainless steels: a review. *Arch Civ Mech Eng* 2022;22(3):129.
- [26] Mohammadzahi S, Mirzadeh H, Sohrabi MJ, Roostaei M, Mahmudi R. Elucidating the effects of cold rolling route on the mechanical properties of AISI 316L austenitic stainless steel. *Mater Sci Eng* 2023:144616.

- [27] Tian J, Deng J, Zhou Y, Chang Y, Liang W, Ma J. Slip behavior during tension of rare earth magnesium alloys processed by different rolling methods. *J Mater Res Technol* 2023;22:473–88.
- [28] Edalati K, Bachmaier A, Beloshenko VA, Beygelzimer Y, Blank VD, Botta WJ, et al. Nanomaterials by severe plastic deformation: review of historical developments and recent advances. *tle Mater. Res. Lett.* 2022;10(4):163–256.
- [29] Bezi Z, Krállics G, El-Tahawy M, Pekker P, Gubicza J. Processing of ultrafine-grained titanium with high strength and good ductility by a combination of multiple forging and rolling. *Mater Sci Eng* 2017;688:210–7.
- [30] Shahriyari F, Shaeri MH, Dashti A, Zarei Z, Noghani MT, Cho JH, et al. Evolution of mechanical properties, microstructure, and texture and of various brass alloys processed by multi-directional forging. *Mater Sci Eng* 2022;831:142149.
- [31] Sakai T, Miura H, Yang X. Ultrafine grain formation in face centered cubic metals during severe plastic deformation. *Mater Sci Eng* 2009;499(1–2):2–6.
- [32] Sitdikov O, Avtokratova E, Markushev M. Development of ultrafine grain structure in an Al–Mg–Mn–Sc–Zr alloy during high-temperature multidirectional isothermal forging. *Met Mater Int* 2021;27:2743–55.
- [33] Shakhova I, Yanushkevich Z, Fedorova I, Belyakov A, Kaibyshev R. Grain refinement in a Cu–Cr–Zr alloy during multidirectional forging. *Mater Sci Eng* 2014;606:380–9.
- [34] Miura H, Yu G, Yang X. Multi-directional forging of AZ61Mg alloy under decreasing temperature conditions and improvement of its mechanical properties. *Mater Sci Eng, A* 2011;528(22–23):6981–92.
- [35] Soleymani V, Eghbali B. Grain refinement in a low carbon steel through multidirectional forging. *J Iron Steel Res Int* 2012;19(10):74–8.
- [36] Xiong Y, Shu KH, Li Y, Chen ZG, Zha XQ, He TT, et al. Excellent strength-ductility synergy in a ultra-high strength Ni–W–Co–Ta medium-heavy alloy by orthogonal rolling. *J Mater Process Technol* 2023;316:117968.
- [37] Yoo JD, Hwang SW, Park KT. Origin of extended tensile ductility of a Fe–28Mn–10Al–1C steel. *Mater Trans A* 2009;40:1520–3.
- [38] Hajiabadi MG, Zamanian M, Soury D. Williamson–Hall analysis in evaluation of lattice strain and the density of lattice dislocation for nanometer scaled ZnSe and ZnSe: Cu particles. *Ceram Int* 2019;45(11):14084–9.
- [39] Ma YF, Xiong Y, Chen ZG, Zha XQ, He TT, Li Y, et al. Microstructure evolution and properties of gradient nanostructures subjected to laser shock processing in 300M ultrahigh-strength Steel. *Steel Res Int* 2021;93(2):2100434.
- [40] Cheng H, Wang HY, Xie YC, Tang QH, Dai PQ. Controllable fabrication of a carbide-containing FeCoCrNiMn high-entropy alloy: microstructure and mechanical properties. *Mater Sci Technol* 2017;33(17):2032–9.
- [41] Xiong Y, Shu KH, Li Y, Chen ZG, Zha XQ, He TT, et al. Deformation temperature impacts on the microstructure evolution and mechanical properties of a novel medium-heavy alloy (MHA). *Mater Sci Eng* 2022;856:144005.
- [42] Wang L, Yang Y, Eisenlohr P, Bieler TR, Crimp MA, Mason DE. Twin nucleation by slip transfer across grain boundaries in commercial purity titanium. *Metall Mater Trans* 2010;41(2):421–30.
- [43] Yoo MH, Morris JR, Ho KM, Agnew SR. Nonbasal deformation modes of HCP metals and alloys: role of dislocation source and mobility. *Metall Mater Trans* 2002;33(3):813–22.
- [44] Gutierrez-Urrutia I, Raabe D. Multistage strain hardening through dislocation substructure and twinning in a high strength and ductile weight-reduced Fe–Mn–Al–C steel. *Acta Mater* 2012;60(16):5791–802.
- [45] Welsch E, Ponge D, Haghghat SMH, Sandlöbes S, Choi P, Herbig M, et al. Strain hardening by dynamic slip band refinement in a high-Mn lightweight steel. *Acta Mater* 2016;116:188–99.
- [46] Hughes DA, Hansen N. The microstructural origin of work hardening stages. *Acta Mater* 2018;148:374–83.
- [47] Taylor I. The mechanism of plastic deformation of crystals. Part I. Theoretical. *Proc. R. Soc. London A Contain. Pap. Math. Phys. Character.* 1934;145(855):362–87.
- [48] Wang F, An ZL, Wang ST, Ji PF, Li B, Jing Q, et al. Effect of different hot deformation temperatures on the microstructure and mechanical properties of high Al/Mn lightweight steel. *J Mater Eng Perform* 2022;31:3799–810.
- [49] Zhu YT, Wu XL. Heterostructured materials. *Prog Mater Sci* 2022:101019.
- [50] Li XL, He Y, Liu LX, Gao XY, Hua K, Wang HF. Overcoming high-temperature strength-ductility trade-off by combination deformation twinning of C11b and D022 superlattices in a Ni–Cr–W/Mo-based superalloy. *Scripta Mater* 2022;220:114931.
- [51] Lu K, Lu L, Suresh S. Strengthening materials by engineering coherent internal boundaries at the nanoscale. *Science* 2009;324(5925):349–52.
- [52] Lu K. Stabilizing nanostructures in metals using grain and twin boundary architectures. *Nat Rev Mater* 2016;1(5):1–13.